# Effective orbital symmetry of CuO: Examination by nonresonant inelastic x-ray scattering

W. B. Wu, N. Hiraoka,* D. J. Huang,† S. W. Huang, and K. D. Tsuei
*National Synchrotron Radiation Research Center, Hsinchu 30076, Taiwan*

Michel van Veenendaal
*Department of Physics, Northern Illinois University, De Kalb, Illinois 60115, USA*
*and Advanced Photon Source, Argonne National Laboratory, 9700 South Cass Avenue, Argonne, Illinois 60439, USA*

Jeroen van den Brink
*Institute for Theoretical Solid State Physics, IFW Dresden, Helmholtzstraße 20, 01069 Dresden, Germany*

Y. Sekio and T. Kimura
*Division of Materials Physics, Graduate School of Engineering Science, Osaka University, Osaka, Japan*
(Received 13 September 2013; published 21 November 2013)

We report on measurements of nonresonant inelastic x-ray scattering (NIXS) to unravel the effective symmetry of Cu $3d$ orbitals in the ground state of CuO. A clear feature of energy loss at about 2 eV exists in the NIXS spectrum, arising from $dd$ excitations; the intensities of these excitations display a pronounced anisotropy. The comparison between the measured angular distributions of scattering and those from theoretical predictions by the tesseral harmonics indicates that, in terms of a hole picture, the lowest-energy $dd$ excitation is the orbital transition $x^2 - y^2 \rightarrow xy$. In addition, the transition $x^2 - y^2 \rightarrow 3z^2 - r^2$ has an energy higher than $x^2 - y^2 \rightarrow yz/zx$, in contrast to a previous interpretation. Our results imply a large Jahn-Teller-like splitting between $x^2 - y^2$ and $3z^2 - r^2$ orbitals. The theory assuming a $C_{4h}$ symmetry explains the angular dependence of the NIXS spectra fairly well, implying that this symmetry is a reasonable approximation. This demonstrates that NIXS can provide important information for modeling of the electronic structure of $d$ ions embedded in a complicated crystal field.

DOI: 10.1103/PhysRevB.88.205129 PACS number(s): 75.85.+t, 78.20.−e, 78.70.Ck

## I. INTRODUCTION

Cupric oxide CuO is a typical Mott insulator, in which copper has the nominal valence of 2+, just as it has in the parent compound of the high-$T_c$ cuprate superconductors.[1–3] It exhibits a wealth of interesting properties, but has a complicated crystal and magnetic structure, distinguishing itself from other transition-metal monoxides (TMO). The crystal structure is monoclinic and characterized by edge-shared plaquette chains of $CuO_2$ (see Fig. 1). In contrast to the other TMO members such as NiO and MnO, a Cu atom is not octahedrally coordinated by six oxygens in CuO but by four oxygens in plane and another four out of plane. (The latter are as far as adjacent coppers.) The Cu valence of 2+ nominally provides a magnetic moment of $1\mu_B$. The crystal shows a spiral magnetic order below $T_{N2} = 230$ K and transforms to an antiferromagnet having a collinear spin order below $T_{N1} = 217$ K. CuO has recently attracted much attention because of its multiferroic properties.[4–15] It shows the magnetoelectric effects at relatively high temperatures: An incommensurate magnetic order is observed between $T_{N2}$ and $T_{N1}$, and this spiral spin order is expected to be linked with a spontaneous dielectric polarization. Furthermore, CuO has been proposed to have orbital currents by a recent resonant x-ray scattering study,[7] though the existence is not necessarily supported by later reports.[16,17] For either case, a theoretical model for a deep understanding of its electronic structure is imperative.[6,8,9,11,18,19] In order to construct an effective model, simple yet realistic parameters are necessary, e.g., those consistent with the local symmetry around a magnetic ion and orbital hybridization with neighbor oxygen atoms. Feedback from experimental data is essential for this purpose.

Inelastic x-ray scattering is a powerful method to probe excited states in matter as a function of momentum transfer $\mathbf{q}$. In particular, nonresonant inelastic x-ray scattering (NIXS) is an effective technique to investigate on-site $d \rightarrow d$ transitions, the so-called $dd$ excitations, which reflect the local symmetry around $d$ ions in a crystal.[20–24] The $dd$ excitation is optically forbidden because it is an even-to-even transition, and thus this excitation is weak in NIXS as long as $\mathbf{q}$ is small. However, as $\mathbf{q}$ increases, the $dd$ excitations lead to a large NIXS intensity with a pronounced anisotropy corresponding to the local symmetry at the $d$-ion site. Unlike resonant inelastic x-ray scattering (RIXS), the large anisotropy is a unique feature of NIXS and its simple scattering process reveals the bare symmetry of the $dd$ excitations. The bulk sensitivity of NIXS facilitates an investigation of the effective orbital symmetry of $d$ ions appropriately describing the crystal field.

In fact, the $dd$ excitations in CuO have previously been investigated,[25,26] but there is a controversy in the interpretation. The first soft-x-ray RIXS experiment[25] revealed a strong feature around 2 eV. This RIXS peak was interpreted as an overlap of several features of excitations described in terms of a hole picture, namely, $x^2 - y^2 \rightarrow xy$ at the lowest energy, then $x^2 - y^2 \rightarrow 3z^2 - r^2$ at a higher energy, and finally $x^2 - y^2 \rightarrow yz/zx$ at the highest energy [see Fig. 2(a)]. A following experiment of the same type with a much improved energy resolution indeed unveiled fine structures indicating the existence of several peaks.[26] However, a recent theoretical study based on the quantum chemistry reports that

 

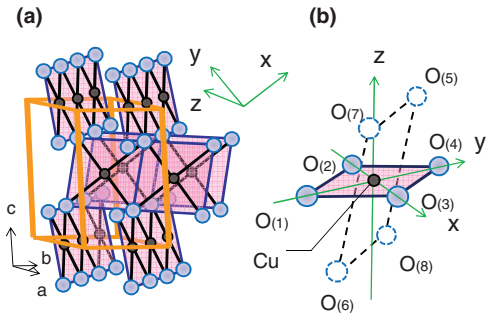


FIG. 1. (Color online) Crystal structure of CuO (a) and local environment around Cu (b). Cu-$O_{(1-4)}$ distances range from 1.90–2.02 Å, while Cu-$O_{(5-8)}$ ranges from 2.78–3.44 Å, depending on temperature: The latter are comparable to adjacent Cu-Cu distances (2.90–3.43 Å).

$x^2 - y^2 \rightarrow 3z^2 - r^2$ has the highest energy [see Fig. 2(b)]. This controversy has remained unsolved.[19]

In this paper, we report on the $dd$ excitations in CuO. We discuss the angular variation of the NIXS line shapes arising from the $dd$ excitations observed around 2 eV in energy loss. From a comparison with theoretical calculations based on tesseral harmonics, given by linear combinations of the spherical harmonics, we have found that the $x^2 - y^2 \rightarrow 3z^2 - r^2$ transition has the highest energy of the $dd$ transitions. We also show that the site symmetry of the $d$ ion is effectively approximated to be $C_{4h}$. This information should be useful for constructing a basic effective model of the electronic structure for CuO because the $d$ orbitals are nicely resolved in this symmetry. So far studies of $dd$ excitations by NIXS are only reported on simple cubic crystals such as NiO and CoO, in which the $O_h$ symmetry is well known to be appropriate. This study attempts to determine the effective symmetry in a highly distorted and complex system.

## II. NIXS MEASUREMENTS

We performed measurements at the Taiwan inelastic x-ray scattering beamline (BL12XU) at SPring-8.[27] X rays from an undulator were first monochromated by a Si(111) double crystal monochromator with a 1.4-eV energy width. The beam was then reflected by Si(400) four-bounce channel-cut crystals so that the energy width was further reduced to 140 meV. The beam was focused by a Pt toroidal mirror to a spot of 80 (vertical) × 120 (horizontal) $\mu$m$^2$. Scattered x rays were

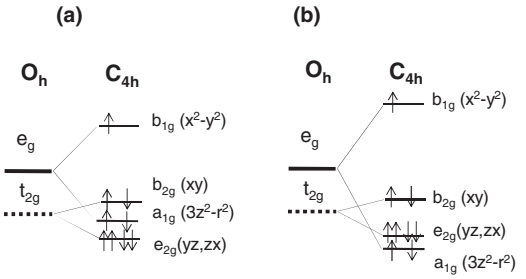


FIG. 2. Energy diagrams of $d$ orbitals in CuO, deduced in a previous experiment (Ref. 25) (a) and in an *ab initio* quantum chemical computation (Ref. 19) (b).

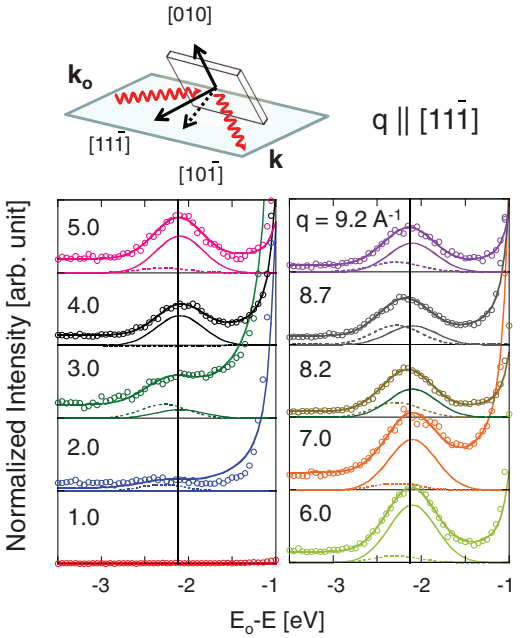


FIG. 3. (Color online) Experimental NIXS spectra (○) as a function of $|\mathbf{q}|$. Thick solid curves are fitted curves. Thin solid (dotted) curves are Gaussian components centered at 2.10 (2.24) eV. The vertical line at 2.10 eV is for a reference.

analyzed by three Si(555) spherically bent crystals positioned along the vertical axis, which is perpendicular to the scattering plane. The photons were finally counted by a Si diode detector. We scanned the incident photon energy ($E$) in the range of 9887–9891.5 eV while the scattered photon energy ($E_0$) was fixed at 9888 eV. A diamond-220 phase plate was installed after the monochromators to obtain a polarization (pre-)factor as uniform as possible. The polarization vector was rotated to the vertical direction; the Stokes parameter for the linear polarization, $P_L$, was 0.85. The overall energy resolution was 250 meV.

A CuO single crystal grown by the floating zone method was cut so that a flat surface was perpendicular to the [10$\bar{1}$] axis. A $|\mathbf{q}|$ scan, namely, a $\theta$-$2\theta$ scan, was performed along [11$\bar{1}$] in an inclined geometry as is shown in Fig. 3. Here $\theta$ and $2\theta$ stand for the sample angle and the scattering angle, respectively. On the other hand, a $\mathbf{q}$-angular scan, namely, a $\theta$ scan, was performed at $|\mathbf{q}| = 8.7$ Å$^{-1}$ by rotating the sample about the [010] axis, where the $\mathbf{q}$ was always on the plane defined by [100] ($a^*$ axis) and [001] ($c^*$ axis). The NIXS spectra were all corrected for the intensity and the polarization of the incident beam and the geometry factor of the self-absorption. A typical count rate was several counts per second. The experiment was performed at room temperature.

Figure 3 summarizes the NIXS spectra measured as a function of $|\mathbf{q}|$, where the $\mathbf{q}$ vector is always parallel to [11$\bar{1}$]. The feature observed at ∼2 eV is enhanced as $\mathbf{q}$ increases; this is a typical behavior of the $dd$ excitation. Figure 4 plots the integrated intensity as a function of $|\mathbf{q}|$, obtained by a fitting analysis (as discussed below). The NIXS intensity maximizes at $|\mathbf{q}| = 6$ Å$^{-1}$ and the peak is centered at $2.1 \pm 0.05$ eV. In the range of $|\mathbf{q}| \geqslant 7$ Å$^{-1}$, the feature shifts toward the high

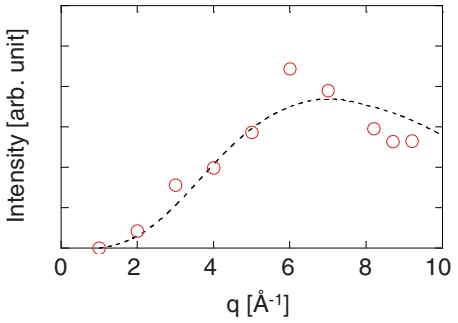


FIG. 4. (Color online) Integrated NIXS intensities (○) as a function of $|\mathbf{q}|$. The dashed curve is a guide to the eye.

energy-loss side (far side from the elastic energy, i.e., left-hand side) by ∼100 meV. This could be due to the propagation nature of the $dd$ excitation such as orbiton or a $\mathbf{q}$ dispersion due to an electron-phonon coupling. This would be an interesting and exciting possibility but the most probable scenario is that there are two excitations having different $|\mathbf{q}|$ dependencies of their intensities. Along this line, we attempted to fit two Gaussians (plus, an exponential decay function for a tail of the elastic line as well as a constant background) to the NIXS spectra. We obtained the best fit when the excitations were at 2.10 and 2.24(±0.05) eV as shown by solid curves and dotted curves in Fig. 3, respectively. The former has the maximum at 6 $\text{Å}^{-1}$ while the latter at 8.7 $\text{Å}^{-1}$. It is possible for different excitations to have different $|\mathbf{q}|$ dependencies as seen in the case of NiO.[24]

Figure 5(a) shows the NIXS spectra measured as a function as the sample angle $\theta$. Here, $\theta = 0^\circ$ means $\mathbf{q}\|[100]$ while $\theta = 80.46^\circ$ is $\mathbf{q}\|[00\bar{1}]$. The $\mathbf{q}$ dependence of the NIXS line shape is remarkable. In addition to the two features mentioned above, another feature is clearly seen at 1.8 eV for a larger $\theta$. Therefore we fit the NIXS spectra by using three Gaussians, and obtained a good fit for Gaussians centered at 1.83, 2.10, and 2.24(±0.05) eV. Moreover, we obtained the best fit by assuming a 250 meV width (instrumental resolution) for the 1.83 eV feature, while a larger width, 380(±100) meV, was assumed for the others.

## III. THEORETICAL APPROACH

The general theory adopted in this study has been discussed in detail in a previous report.[22] We demonstrate how the theory is applied to CuO in the following. NIXS excited by x rays of a vector potential $\mathbf{A}$ involves the interaction

$$\frac{e^2}{2m}\mathbf{A}^2 = \frac{e^2}{2m}(\mathbf{e}'\cdot\mathbf{e})e^{i\mathbf{q}\cdot\mathbf{r}}, \tag{1}$$

where $\mathbf{e}$ and $\mathbf{e}'$ are the polarization vectors of incident and scattered x rays, respectively. One can expand the exponent in Eq. (1) in terms of Bessel functions and tesseral harmonics,

$$e^{i\mathbf{q}\cdot\mathbf{r}} = \sum_{LM}(2L+1)i^L j_L(qr)Z_M^{(L)}(\hat{\mathbf{q}})Z_M^L(\hat{\mathbf{r}}), \tag{2}$$

where $M = -L, -L+1, \ldots, L$, and $j_L$ is a Bessel function of order $L$. The functions $Z_M^{(L)}(\hat{\mathbf{q}})$ are known as tesseral harmonics, which are given by linear combinations of the spherical harmonics. For transition-metal compounds, the $M$ values are −2, −1, 0, 1, and 2, corresponding to the $3d$ orbitals $d_{xy}$, $d_{yz}$, $d_{3z^2-r^2}$, $d_{xz}$, and $d_{x^2-y^2}$, respectively. In addition, the effective transition operator is

$$\rho_{\mathbf{q}} = \sum_L A_L(q)Z_M^{(L)}(\hat{\mathbf{q}})w_M^L, \tag{3}$$

consisting of a one-particle transition operator $w_M^L$ probed by $\mathbf{q}$ through a reduced (radial part) matrix element $A_L(q)$ and an angular dependence $Z_M^{(L)}(\hat{\mathbf{q}})$. Of the summation over $L$ only the values 0 (monopolar), 2 (quadrupolar), and 4 (hexadecapolar)

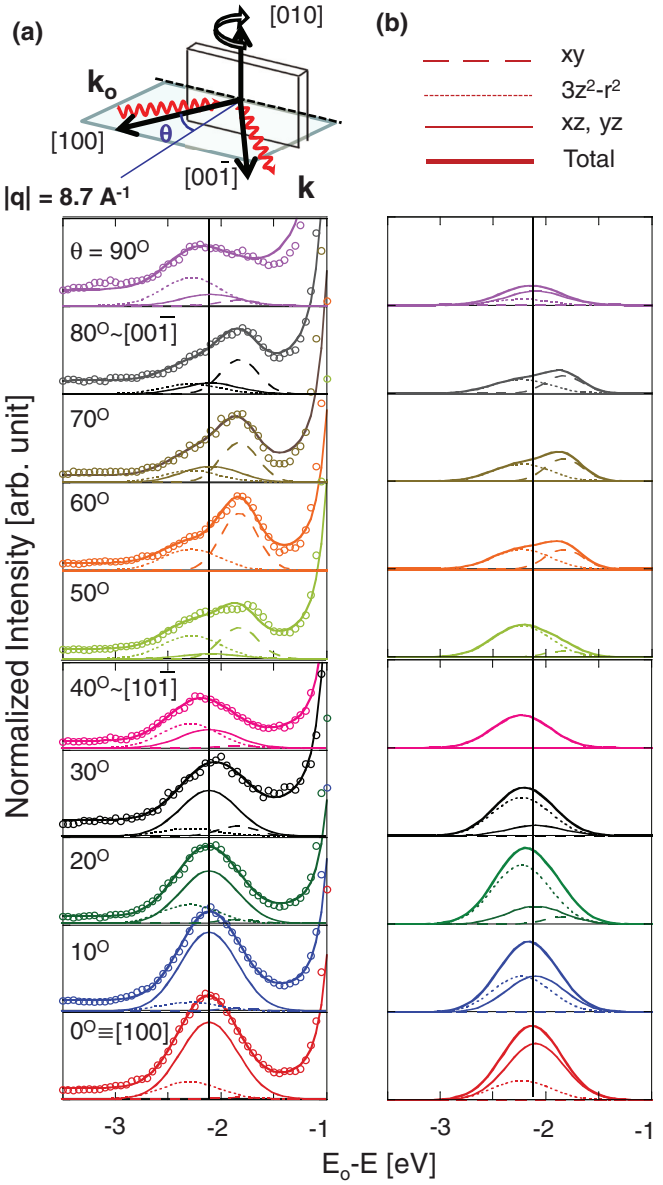


FIG. 5. (Color online) (a) Experimental NIXS spectra (○) as a function of $\theta$ or the sample orientation. The [100] axis is at $\theta = 0^\circ$ while the [00$\bar{1}$] axis is at $\theta = 80.45^\circ$. Thick solid curves are fitted curves. Thin solid, dotted, and broken curves are Gaussian components centered at 2.10, 2.24, and 1.83 eV, respectively. The vertical line at 2.10 eV is for a reference. (b) Angular variation of NIXS specta, reproduced by tessal harmonics: Positions and widths for three features are fixed at those obtained by the experiment, while the intensity variations are given by the theory.

remain, but the $L = 0$ excitation only contributes the elastic scattering. The angular dependence of the scattering between orbitals $m$ and $m'$ is $U_{mm'} = \langle m'|\rho_{\mathbf{q}}|m\rangle$, sensitive to the detailed nature of the ground state. For inelastic scattering due to local $dd$ transitions in transition-metal systems, the selection rule which makes $U_{mm'}$ nonzero is

$$m' = \mathrm{sgn}(mM)|m \pm M|. \quad (4)$$

This selection rule and the symmetry can help us obtain the ground-state information. Now we consider a $Cu^{2+}$ ion in $C_{4h}$ symmetry for the quadrupolar $L = 2$ transition; the ground state is $\underline{d}_{x^2-y^2}$, i.e., $m = 2$, where the underline indicates holes. Let us consider the case of $M = 2$ to show how the different orientations of the plaquettes and the interference between the different channels can affect the angular distribution. For $M = 2$, scattering occurs only to $m = 0$, or the $\underline{d}_{3z^2-r^2}$ orbital, since $m = 4$ does not exist. The angular dependence is given by the tesseral harmonic which, for quadrupolar transitions ($L = 2$) with $M = 2$, appears like an $d_{x^2-y^2}$ orbital with respect to the $CuO_4$ plaquette. Because the crystal structure of CuO is complex with CuO chains along the [110] and [1$\bar{1}$0] [see Fig. 6(a)], the combined angular distribution of the scattering driven by $w_2^2$ is composed of $\underline{d}_{x^2-y^2} \rightarrow \underline{d}_{3z^2-r^2}$ transitions in $CuO_4$ plaquettes of two different orientations, as plotted in Figs. 6(b) and 6(c). We sum them to obtain the angular distribution of the $L = 2$ transition amplitude [Fig. 6(d)] in an incoherent way since they do not interfere with each other. A similar procedure is applied to the hexadecapolar transitions ($L = 4$): The $\underline{d}_{x^2-y^2} \rightarrow \underline{d}_{3z^2-r^2}$ transition is possible with $M = 2$. The angular distribution of the scattering driven by $w_2^4$ does not appear like a $d$ orbital anymore but like a $g$ orbital [Fig. 6(e)]. These $L = 2$ and $L = 4$ transitions interfere with each other when taking a square of the transition

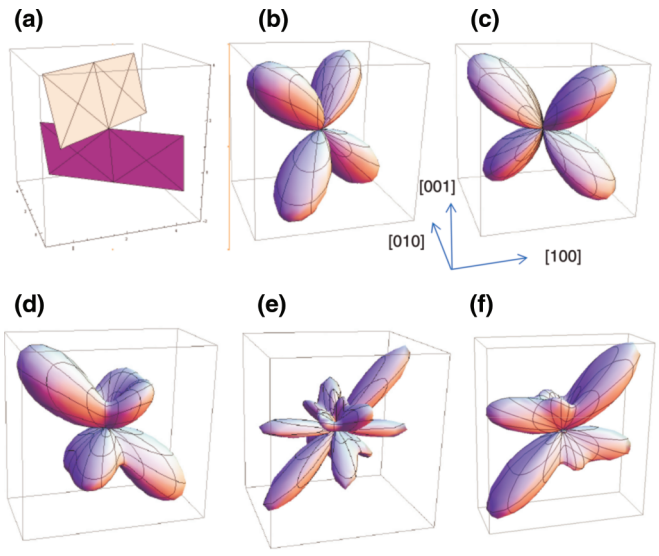


FIG. 6. (Color online) (a) Configuration of $CuO_4$ plaquettes along the [110] and [1$\bar{1}$0] directions. (b), (c) Theoretical angular distributions of quadrupole channel ($L = 2, M = 2$) in the $x^2 - y^2 \rightarrow 3z^2 - r^2$ transition in a plaquette in both directions, and (d) the sum of them. (e) Same computation for the hexadecapole channel ($L = 4$, $M = 2$). (f) Intensity distribution of the $x^2 - y^2 \rightarrow 3z^2 - r^2$ transition after interference between the $L = 2$ and $L = 4$ channels.

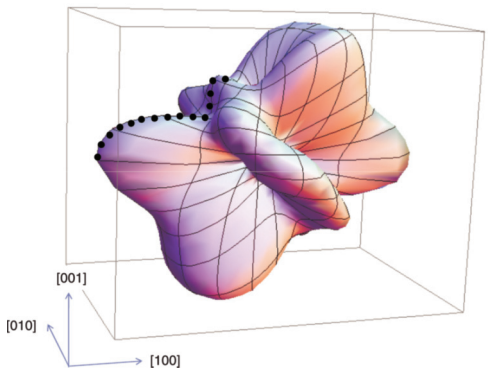


FIG. 7. (Color online) Total intensity distribution over all the transitions for $x^2 - y^2 \rightarrow xy, xz(yz)$, and $3z^2 - r^2$. The thick, dotted curve indicates the region of comparison plotted in Fig. 8.

amplitudes, and we then obtain the intensity distribution of the inelastic scattering as plotted in Fig. 6(f). We repeat the same calculation for the $\underline{d}_{x^2-y^2} \rightarrow \underline{d}_{xy}$ transition and for the $\underline{d}_{x^2-y^2} \rightarrow \underline{d}_{yz/zx}$ transition. Figure 7 displays the total intensity distribution for all the inelastic features in a 3D $\mathbf{q}$ space.

## IV. DISCUSSIONS

Figure 8 compares the theoretical intensity distributions of the total excitations (thick, solid curve) with the experimental ones (circles). The comparison is made on the plane including the [100] and [00$\bar{1}$] axes, as indicated by a thick, dottted curve in Fig. 7. Overall, good agreement is achieved. We have attempted to decompose the excitation features using a fitting scheme described previously [see Fig. 5(a)]. The feature at 1.8 eV is nicely resolved by the fitting, while those at 2.1 and 2.2 eV are difficult to decompose because their energy positions are too close, limiting a quantitative analysis. Therefore, the decomposed intensities only of the 1.8 eV feature are shown along with the total intensities in Fig. 8. The calculation agrees reasonably well with the observed intensity variation for different directions of $\mathbf{q}$. This is clear evidence that the 1.8-eV feature is due to the transition of $x^2 - y^2 \rightarrow xy$. These agreements indicate the assumed $C_{4h}$ symmetry is a good approximation for the $d$ orbitals.

Another issue is what transitions the 2.1- and 2.2-eV features correspond to. According to a previous report of soft x-ray RIXS, $x^2 - y^2 \rightarrow yz/zx$ has a higher energy, and thus the 2.2-eV feature would be due to the transition to $yz/zx$, while the 2.1-eV feature would be due to the transition to $3z^2 - r^2$. However, our data show the opposite: The 2.2-eV feature is associated with $3z^2 - r^2$, while the 2.1-eV feature is associated with the other. As seen in Fig. 5(a), the feature of $dd$ excitation shifts toward the high-energy side (far side from the elastic energy, i.e., the left-hand side) near [10$\bar{1}$]. Along this axis, the $dd$ excitation intensity is purely occupied by the $3z^2 - r^2$ component as seen in Fig. 8. This fact strongly suggests that the transition of $x^2 - y^2 \rightarrow 3z^2 - r^2$ has larger energy than the others, supporting the prediction by recent *ab initio* quantum chemical calculations.[19]

The theory used here is based on the orbital symmetry and does not predict the energy of the excitations. Nonetheless, the angular variation can be reproduced by substituting the

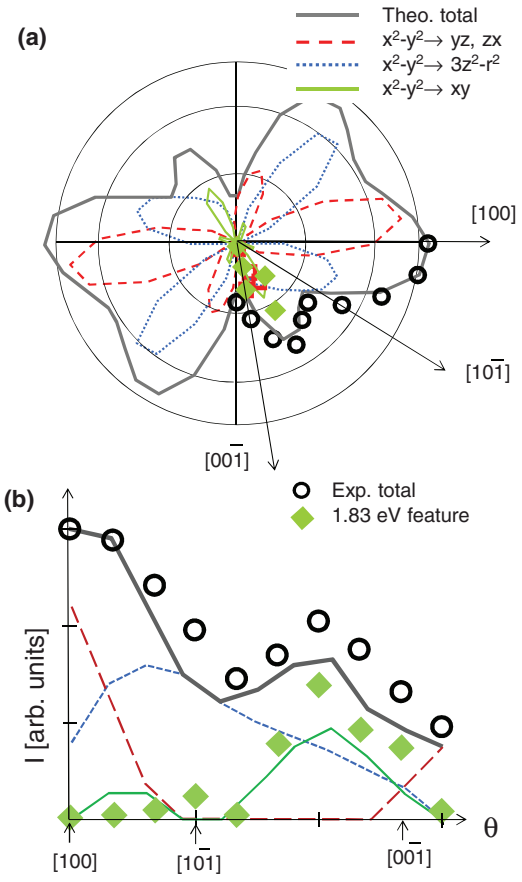


FIG. 8. (Color online) Polar plot (a) and linear plot (b) of theoretical intensity distribution: Thin solid, broken, and dotted curves are the intensity distributions for the $x^2 - y^2 \rightarrow xy$, $yz(zx)$, and $3z^2 - r^2$ transitions, respectively. The thick solid curve is for the total intensities summed over all the transitions, compared with the experiment (circles). Diamonds are for decomposed intensities of the 1.8 eV feature.

parameters obtained from the experiment. Figure 5(b) shows the theoretical variation of the spectrum as a function of the **q** direction. Here, 1.83, 2.10, and 2.24 eV are used as the energies of the transitions to $xy$, $yz/zx$, and $3z^2 - r^2$, with a width of 250 meV for the first one and a width of 380 meV for the others. A satisfactory agreement between the experiment [Fig. 5(a)] and the theory [Fig. 5(b)] has been reached. In particular, the theory reproduces well the experimental observations of the spectral weight shifting toward the low-energy side (near side to the elastic energy, i.e., the right-hand side) near [00$\bar{1}$] and a slight shift toward the high-energy side near [10$\bar{1}$].

As described above, the tesseral-harmonics-based theory for a square plaquette reproduces the general trend of the angular dependence of the NIXS spectra satisfactorily well, indicating that a $C_{4h}$ symmetry is a good approximation for the $d$ orbitals even though the real symmetry is much lower ($C_i$ or $C_1$). If the influence from the off-plane oxygen (and/or copper) ions were large, as seen in Fig. 1(b), a low symmetry such as $C_{2v}$, $C_i$, or $C_1$, would have to be adopted even for an exactly square plaquette. Such an influence is, however, minor, and thus $C_{4h}$ becomes a good approximation, making the problem much simpler.

Probably, another useful symmetry is $D_{4h}$, in which the degeneracy of $yz$ and $zx$ is lifted. This symmetry would certainly lead to a better agreement in the fitting analysis since it effectively introduces one more variable parameter as the excitation energy. However, there is no real necessity to assume the $D_{4h}$ symmetry in explaining our data because we only see three excitation features. In fact, the quantum chemistry theory predicts that the splitting of the $yz$ and $zx$ orbitals is as small as 60 meV.[19] A further lower symmetry would need to be assumed only if we attempt to achieve a quantitative agreement, rather than the present qualitative agreement. For example, the theory underestimates the intensity of the feature at 1.8 eV (associated with $xy$). Also, the theory presumably overestimates that at 2.2 eV ($3z^2 - r^2$) at $\theta \sim 20^\circ$, leading to a peak shift larger than the experiment. Furthermore, the evaluated widths for the 2.1- and 2.2-eV features are much broader than the instrumental resolution. Such quantitative disagreements may be addressed if one assumes a lower symmetry and carefully resolves the $d$ orbitals which can be tangled in a complicated way because of the low symmetry. It is important to pursue better agreement using a more precise theory in the future, though in this study we have adopted a simple and flexible model to examine the effective site symmetry.

## V. SUMMARY

We investigated the $dd$ excitations of CuO by using nonresonant inelastic x-ray scattering. A NIXS feature arising from the $dd$ excitations about 2 eV in energy loss consists of several peaks displaying a strong anisotropy of the intensity. Comparing NIXS data with a theory based on the tesseral harmonics, we show that the excitation of the lowest energy is the $x^2 - y^2 \rightarrow xy$ transition. Furthermore, we suggest that the $x^2 - y^2 \rightarrow 3z^2 - r^2$ transition has a higher energy than that of $x^2 - y^2 \rightarrow yz/zx$, implying a large Jahn-Teller-like splitting between the $x^2 - y^2$ and the $3z^2 - r^2$ levels. The theory reproduces a general trend of the angular variation of the inelastic spectra fairly well. This observation indicates that the $C_{4h}$ symmetry is a good approximation for the local crystal field around the $d$ ion, despite the much lower orbital symmetry in the real crystal, $C_i$ (or $C_1$). Although we mainly discussed the **q**-angular dependence of $dd$ excitations in this study, the $|\mathbf{q}|$ dependence, however, should include valuable information such as a radial extent of the $d$ orbitals as well as the orbital hybridization with $p$ orbitals of oxygen. The next goal will be to extract such information by integrating the radial part of the wave function to the theory.

*Note added.* A report utilizing the same technique on the same sample has appeared recently.[28] The temperature effect is mainly investigated, though the symmetry analysis is little performed in the report. There is no conflict with our conclusion.

## ACKNOWLEDGMENTS

We thank the staffs of NSRRC and JASRI/SPring-8 for technical support. The work is supported in part by the National Science Council of Taiwan under Grant No. NSC-

100-2112-M-213-05-MY3, and also by the US Department of Energy (DOE), DE-FG02-03ER46097, and NIU's Institute for Nanoscience, Engineering, and Technology. Work at Argonne National Laboratory was supported by the US DOE, Office of Science, Office of Basic Energy Sciences, under Contract No. DE-AC02-06CH11357. The experiment was performed under the approval of JASRI/SPring-8 and NSRRC, Taiwan (Proposal No. 2008B4256/2008-2-088).

*hiraoka@spring8.or.jp
†djhuang@nsrrc.org.tw

[1] J. Ghijsen, L. H. Tjeng, J. van Elp, H. Eskes, J. Westerink, G. A. Sawatzky, and M. T. Czyzyk, Phys. Rev. B **38**, 11322 (1988).
[2] H. Eskes, L. H. Tjeng, and G. A. Sawatzky, Phys. Rev. B **41**, 288 (1990).
[3] H. Hayashi, Y. Udagawa, W. A. Caliebe, and C. C. Kao, Phys. Rev. B **66**, 033105 (2002).
[4] T. Kimura, Y. Sekio, H. Nakamura, T. Siegrist, and A. P. Ramirez, Nat. Mater. **7**, 291 (2008).
[5] W. B. Wu, D. J. Huang, J. Okamoto, S. W. Huang, Y. Sekio, T. Kimura, and C. T. Chen, Phys. Rev. B **81**, 172409 (2010).
[6] J. Sirker, Phys. Rev. B **81**, 014419 (2010).
[7] V. Scagnoli, U. Staub, Y. Bodenthin, R. A. de Souza, M. García-Femández, M. Garganourakis, A. T. Boothroyd, D. Prabhakaran, and S. W. Lovesey, Science **332**, 696 (2011).
[8] G. Giovannetti, S. Kumar, A. Stroppa, J. van den Brink, S. Picozzi, and J. Lorenzana, Phys. Rev. Lett. **106**, 026401 (2011).
[9] P. Tolédano, N. Leo, D. D. Khalyavin, L. C. Chapon, T. Hoffmann, D. Meier, and M. Fiebig, Phys. Rev. Lett. **106**, 257601 (2011).
[10] P. Babkevich, A. Poole, R. D. Johnson, B. Roessli, D. Prabhakaran, and A. T. Boothroyd, Phys. Rev. B **85**, 134428 (2012).
[11] G. Jin, K. Cao, G. C. Guo, and L. He, Phys. Rev. Lett. **108**, 187205 (2012).
[12] R. Villarreal, G. Quirion, M. L. Plumer, M. Poirier, T. Usui, and T. Kimura, Phys. Rev. Lett. **109**, 167206 (2012).
[13] G. Quirion and M. L. Plumer, Phys. Rev. B **87**, 174428 (2013).
[14] K. Y. Choi, W. J. Lee, A. Glamazda, P. Lemmens, D. Wulferding, Y. Sekio, and T. Kimura, Phys. Rev. B **87**, 184407 (2013).
[15] M. Heinemann, B. Eifert, and C. Heiliger, Phys. Rev. B **87**, 115111 (2013).
[16] S. Di Matteo and M. R. Norman, Phys. Rev. B **85**, 235143 (2012).
[17] Y. Joly, S. P. Collins, S. Grenier, H. C. N. Tolentino, and M. De Santis, Phys. Rev. B **86**, 220101(R) (2012).
[18] M. A. van Veenendaal and G. A. Sawatzky, Phys. Rev. B **49**, 3473 (1994).
[19] H. Y. Huang, N. A. Bogdanov, L. Siurakshina, P. Fulde, J. van den Brink, and L. Hozoi, Phys. Rev. B **84**, 235125 (2011).
[20] B. C. Larson, J. Z. Tischler, W. Ku, C. C. Lee, O. D. Restrepo, A. G. Eguiluz, P. Zschack, and K. D. Finkelstein, Phys. Rev. Lett. **99**, 026401 (2007).
[21] M. W. Haverkort, A. Tanaka, L. H. Tjeng, and G. A. Sawatzky, Phys. Rev. Lett. **99**, 257401 (2007).
[22] M. van Veenendaal and M. W. Haverkort, Phys. Rev. B **77**, 224107 (2008).
[23] C. C. Lee, H. C. Hsueh, and W. Ku, Phys. Rev. B **82**, 081106(R) (2010).
[24] N. Hiraoka, M. Suzuki, K. D. Tsuei, H. Ishii, Y. Q. Cai, M. W. Haverkort, C. C. Lee, and W. Ku, Europhys. Lett. **96**, 37007 (2011).
[25] G. Ghiringhelli, N. B. Brookes, E. Annese, H. Berger, C. Dallera, M. Grioni, L. Perfetti, A. Tagliaferri, and L. Braicovich, Phys. Rev. Lett. **92**, 117406 (2004).
[26] G. Ghiringhelli, A. Piazzalunga, X. Wang, A. Bendounan, H. Berger, F. Bottegoni, N. Christensen, C. Dallera, M. Grioni, J.-C. Grivel *et al.*, Eur. Phys. J. Spec. Top. **169**, 199 (2009).
[27] Y. Q. Cai, P. Chow, C. C. Chen, H. Ishii, K. L. Tsang, C. C. Kao, K. S. Liang, and C. T. Chen, in *Synchrotron Radiation Instrumentation: Eighth International Conference*, edited by T. Warwick *et al.*, AIP Conf. Proc. No. 705 (AIP, Melville, NY, 2004), p. 340.
[28] S. Huotari, L. Simonelli, C. J. Sahle, M. M. Sale, R. Verbeni, and G. Monaco, arXiv:1310.6730.